Supporting Information

Metal-organic framework (MOF) derived flower-shaped CoSe$_2$ nanoplates as a superior bifunctional electrocatalyst for both oxygen and hydrogen evolution reaction

Nachiketa Sahu,[abc] Jiban K. Das[abc] and J. N. Behera*[abc]

[a]School of Chemical Sciences, National Institute of Science Education and Research (NISER), Khordha 752050, Odisha, India

[b]Homi Bhabha National Institute (HBNI), Mumbai, India

[c]Centre for Interdisciplinary Sciences (CIS),NISER,752050, Jatni, Odisha, India

E-mail: jnbehera@niser.ac.in

➢ **Procedure for the removal of Fe from 1 M KOH:**

Firstly, the Co $(OH)_2$ was synthesized by adding 0.5 g of $Co(NO_3)_2$. $6H_2O$ to 1 ml of deionized water followed by 5 ml of 0.1 M KOH solution, respectively. The solution mixture was centrifuged and washed with deionized water four times. The fourth time washed Co $(OH)_2$ was used to purify 1 M KOH solution. 12 mL of 1 M KOH taken in a 15 mL centrifuge tube followed by the addition of as-prepared $Co(OH)_2$ and shaken well to absorb the iron impurities. Further, the brown-colored precipitate was separated by centrifugation at 3000 rpm to collect the purified KOH solution. By continuing the purification process, the as decanted 1 M KOH was washed repeatedly four times. After the purification process, the KOH solution was used as the iron-free supporting electrolyte for oxygen evolution reaction.

➢ **Quantification of evolved oxygen (Faradaic Efficiency)**

During the OER process, gas bubbles evolution was noticed on the sample modified glassy carbon electrode (GCE). Since it is an anodic scan, so oxidation of water is expected to produce molecular oxygen. Therefore the rotating ring disk electrode (RRDE) method has been used to detect evolved oxygen at the platinum ring electrode to quantify the efficiency of the active catalyst (Fig. S12). Herein, the glassy carbon disk electrode (geometrical surface area: 0.19 cm^2) was coated with the active catalyst (mass loading, 0.25 mg cm^{-2}) and sweep from 0.0 V to +0.9 V (vs. Hg/HgO) at 5 mV/s and a rotation rate of 167.52 rad/s. At the same time, a static potential (-0.5 V vs. Hg/HgO) was applied to the Pt ring electrode. As per the mechanism, the oxygen evolved at the rotating disk electrode (equation 1) swept over the Pt ring where it was reduced (equation 2) at the applied potential under mass transport controlled conditions,

$$4OH^- \rightarrow O_2 + 2H_2O + 4e^-$$ .... (1)

$$O_2 + 2H_2O + 2e^- \rightarrow H_2O_2 + 2OH^-$$ .... (2)
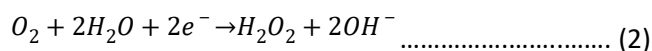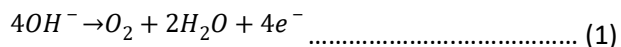
After that, the Faradaic efficiency (FE) has been calculated as per the following equation,

$$Faradaic\ Efficiency = \frac{I_R \times n_D}{I_D \times n_R \times N_{CL}} \quad\text{.................................}\ (3)$$

Here, I_R is the ring current, I_D is the disk current, n_D and n_R are the number of electrons transferred during the evolution and reduction of oxygen (here, both reactions involved a 4e-process). The term, N_{CL}, is the collection efficiency of the RRDE used (for our electrode, it is 0.249). The observed ratio of the ring limiting current to the disk limiting current is the collection efficiency (N_{CL}) of the used RRDE electrode. The collection efficiency of the rotating ring-disk electrode was determined by the ratio of ring and disk current in 0.001 M $K_3Fe(CN)_6$ containing 1 M of KOH solution, which was 0.249. The reduction of ferricyanide $[Fe(CN)_6]^{3-}$ to ferrocyanide $[Fe(CN)_6]^{4-}$ occurs at the disk electrode, whereas ferrocyanide is oxidized to ferricyanide at the ring electrode.
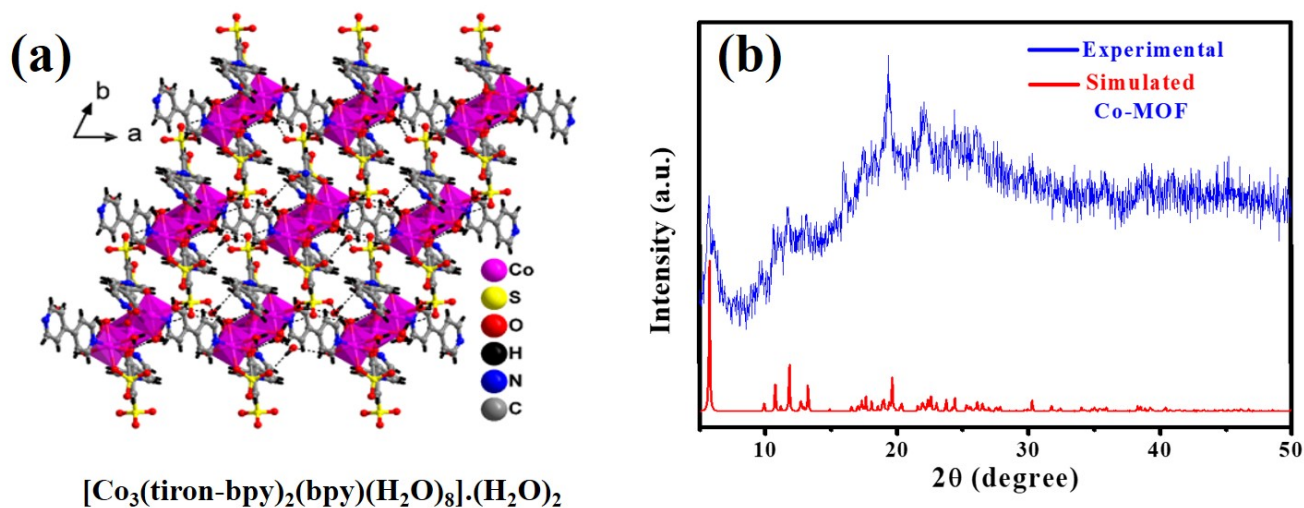

$[Co_3(tiron-bpy)_2(bpy)(H_2O)_8].(H_2O)_2$

Fig. S1 (a) Crystal structure of the 1D Co-MOF growing along *c*-axis and (b) Powder X-ray diffraction pattern for Co-MOF.
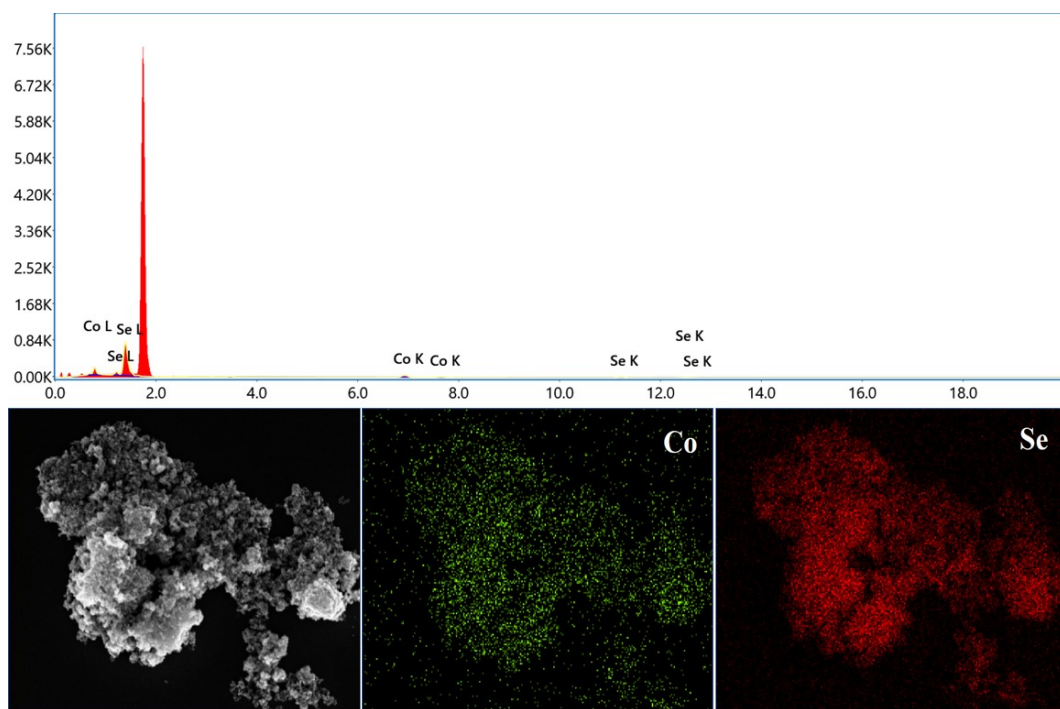
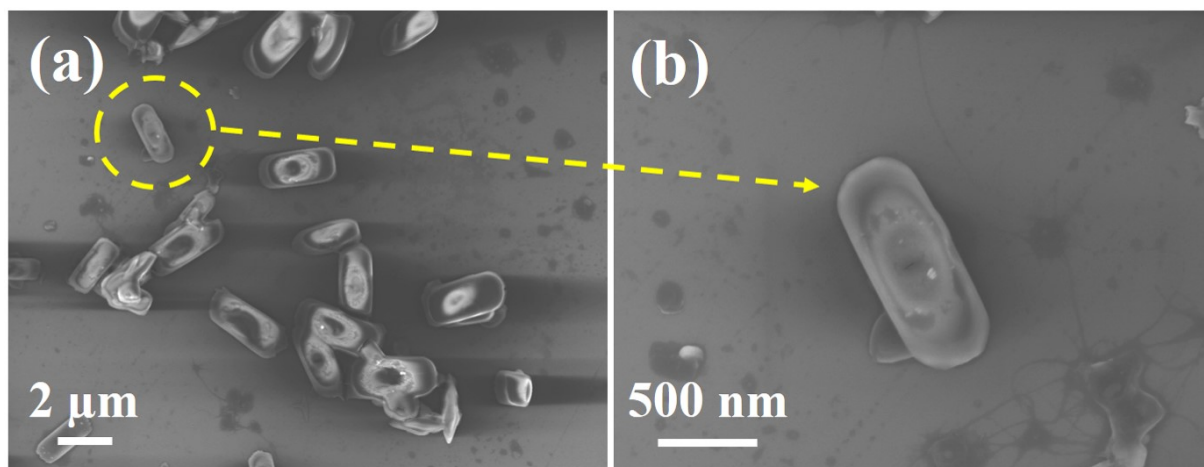**Fig. S2** Energy dispersive X-ray analysis of the MOF-derived CoSe$_2$ (MOF-D CoSe$_2$).

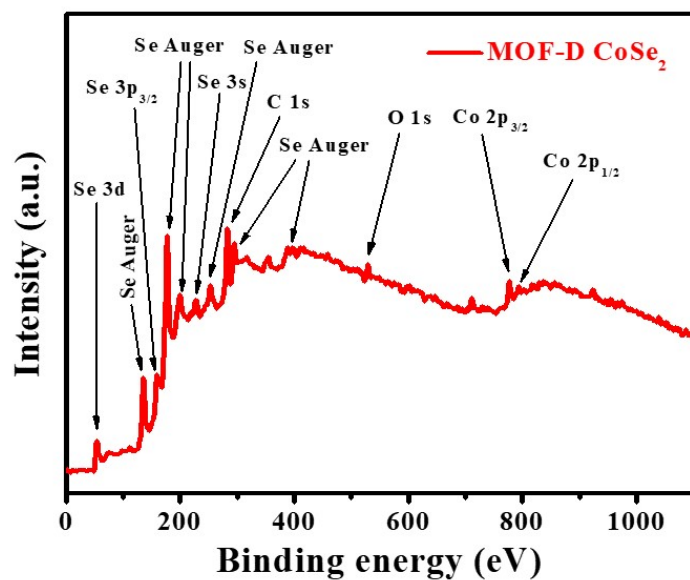**Fig. S3** (a), (b) FESEM image of Co-MOF at different magnifications.

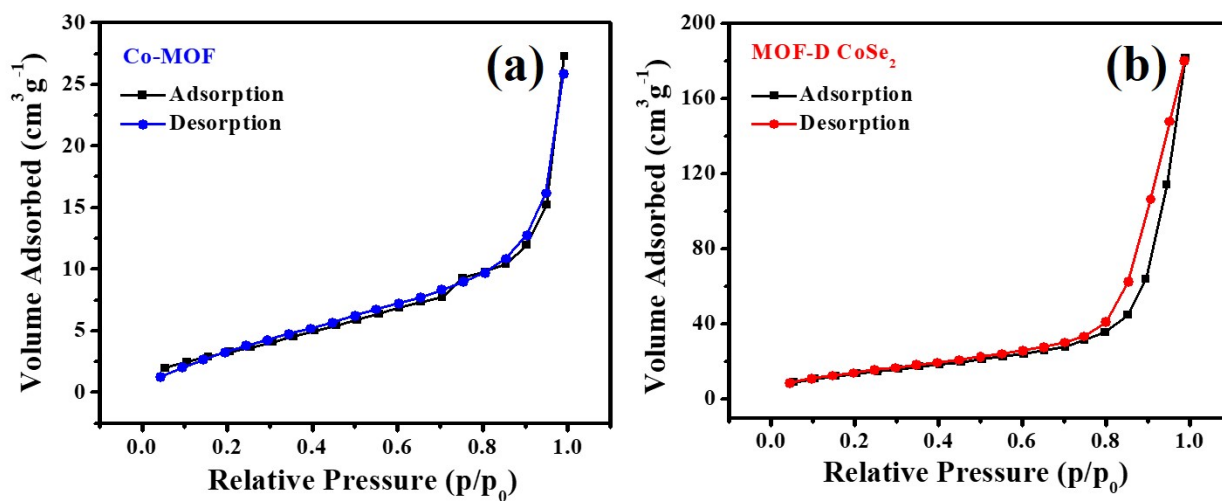**Fig. S4** High-resolution full scan XPS survey of MOF-D CoSe$_2$.

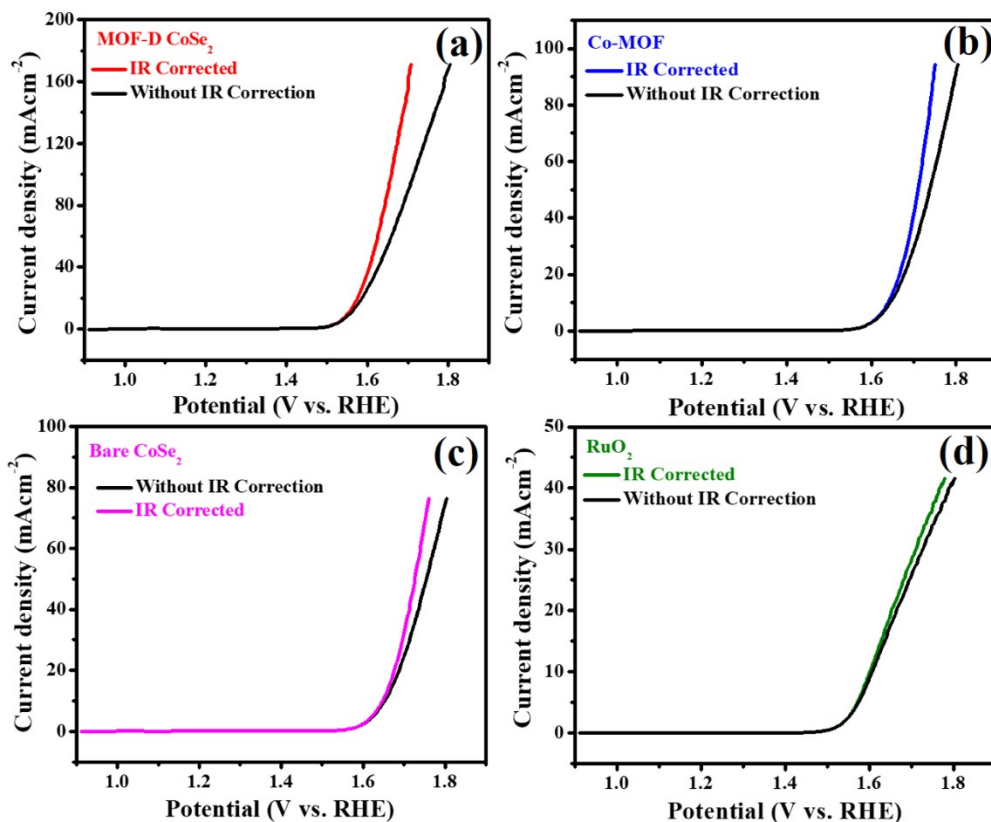**Fig. S5** BET analysis of (a) Co-MOF and (b) MOF-D-CoSe$_2$.

Fig. S6 LSV plots of (a) MOF-D $CoSe_2$, (b) bare $CoSe_2$, (c) Co-MOF and (d) RuO_2 for oxygen evolution reaction before and after *iR* compensation. All the LSVs data are presented at a sweep rate of 5 mV/s in 1 M KOH.
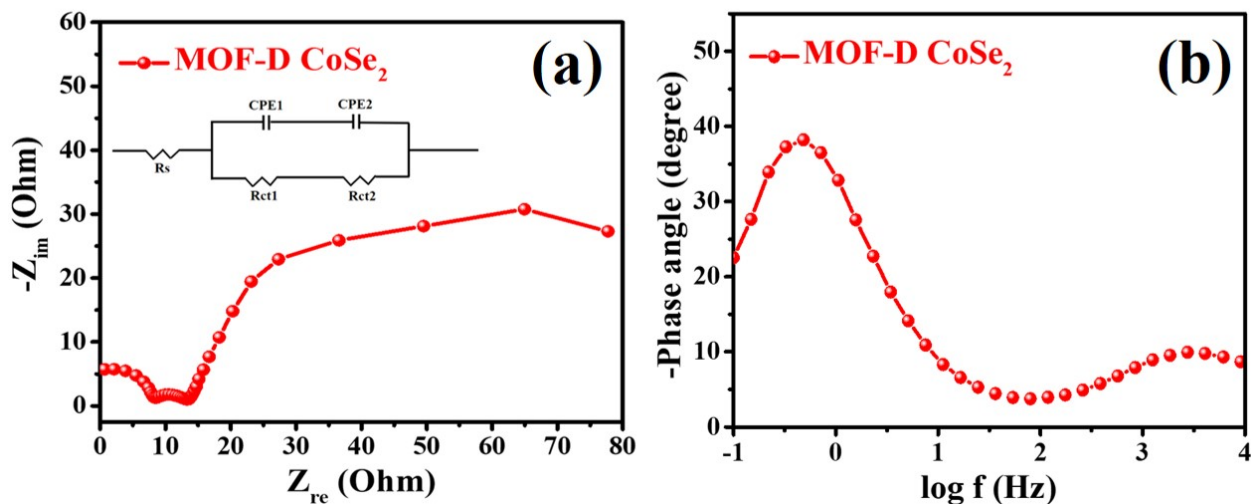
Fig. S7 (a) The equivalent circuit diagram of MOF-D CoSe$_2$ fitted to the obtained impedance result and (b) is the bode plot corresponds to the time constant for OER.
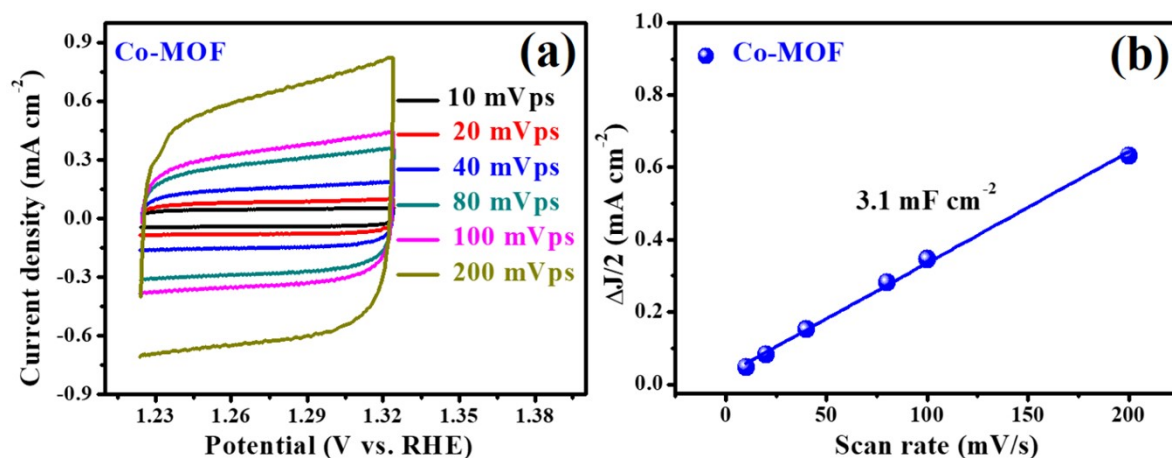

Fig. S8 (a) Cyclic voltammograms for Co-MOF in 1 M KOH at various sweep rates (from 10 to 200 mV/s) and (b) the plot of sweep rate vs. current density at 1.27 V vs. RHE to estimate the ECSA.
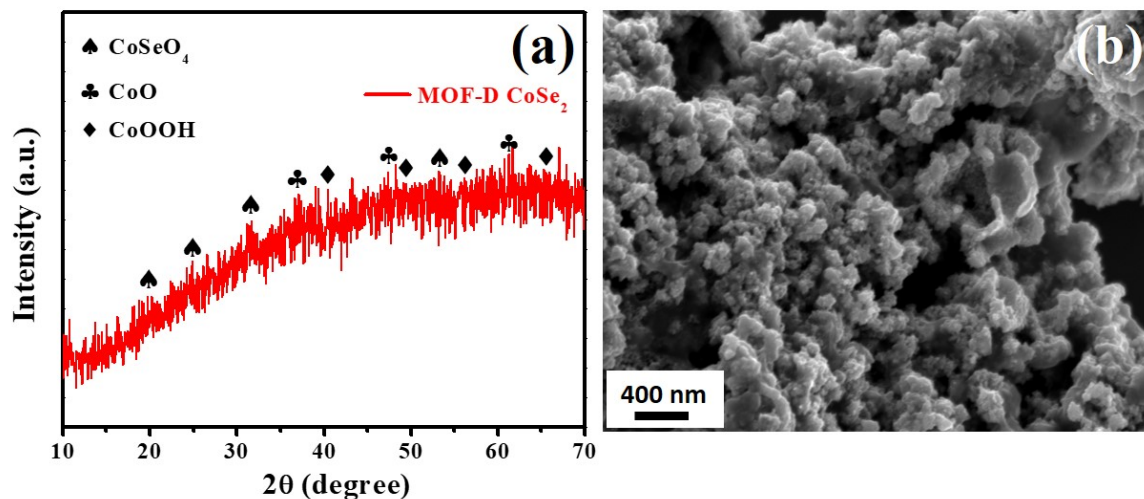

Fig. S9 (a) PXRD and (b) FESEM picture of the MOF-D CoSe$_2$ electrocatalyst after stability test.
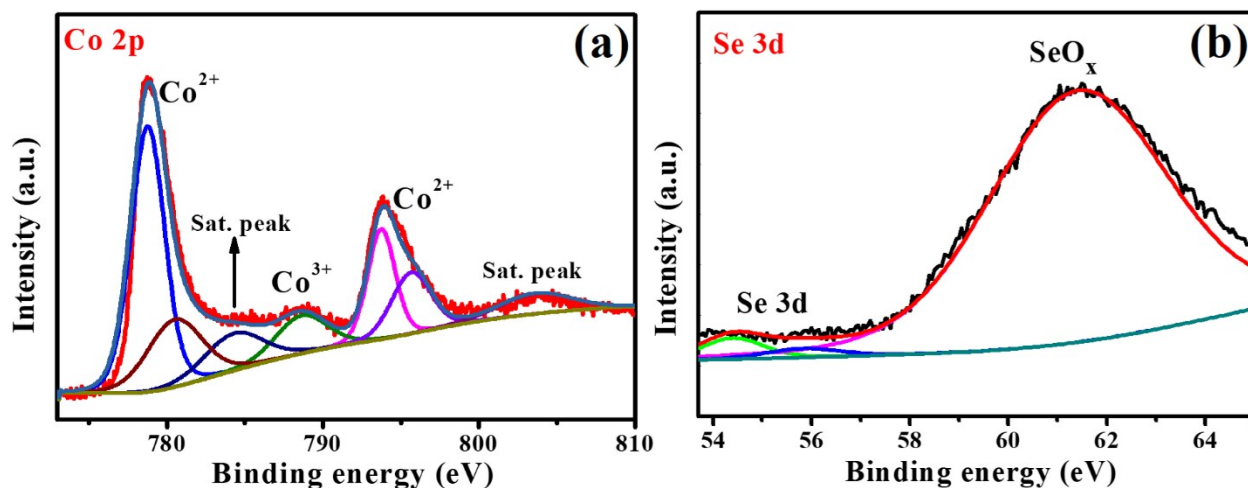
Fig. S10 (a, b) High-resolution XPS study of MOF-D CoSe$_2$ after 16 h of long-term stability test in 1 M KOH.
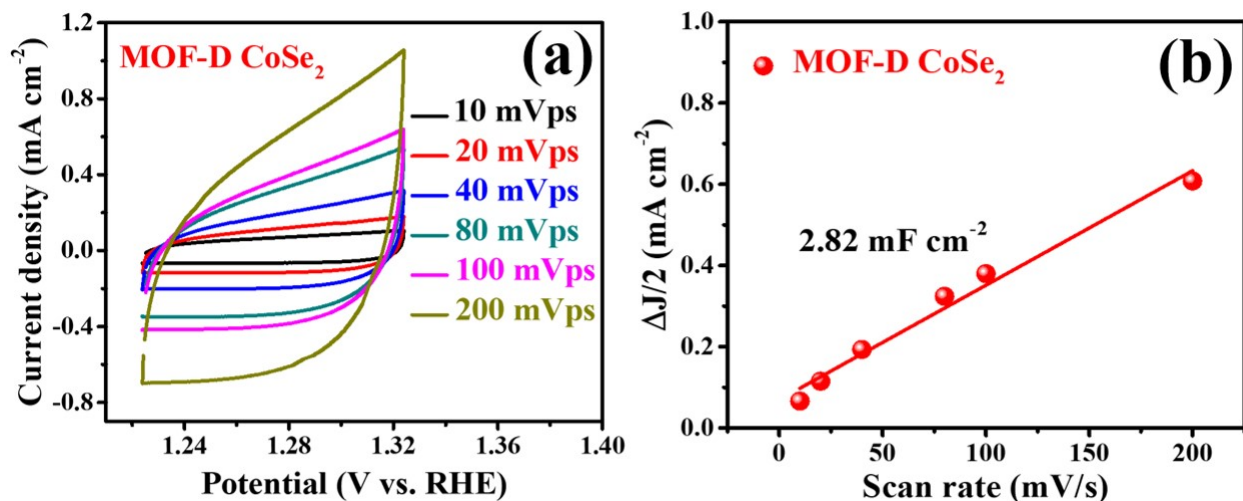

Fig. S11 (a) Post cyclic voltammograms for MOF-D CoSe$_2$ in 1 M KOH at different scan rates (from 10 to 200 mV/s) and (b) the graph of current density at 1.27 (V vs. RHE) vs. scan rates to calculate the double-layer capacitance (C_{dl}).
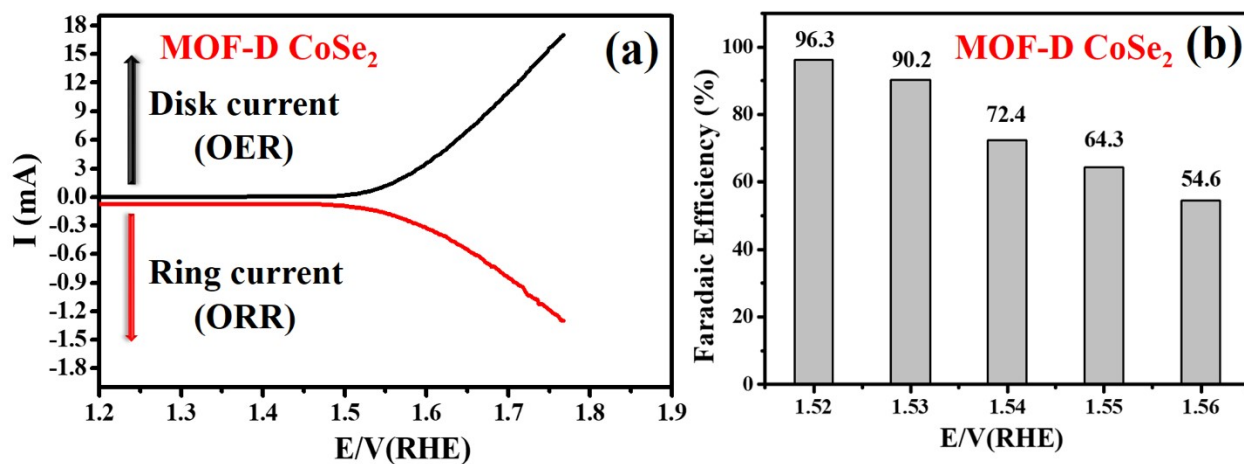
Fig. S12 (a, b) Rotating ring disk electrode voltammograms for MOF-D $CoSe_2$ in 1 M KOH electrolyte at a scan rate of 5 mV/s and a rotation rate of 167.52 rad/sec. The platinum ring electrode was set at -0.5 V (vs. Hg/HgO) to detect the oxygen, evolving from the sample modified glassy carbon disk electrode.
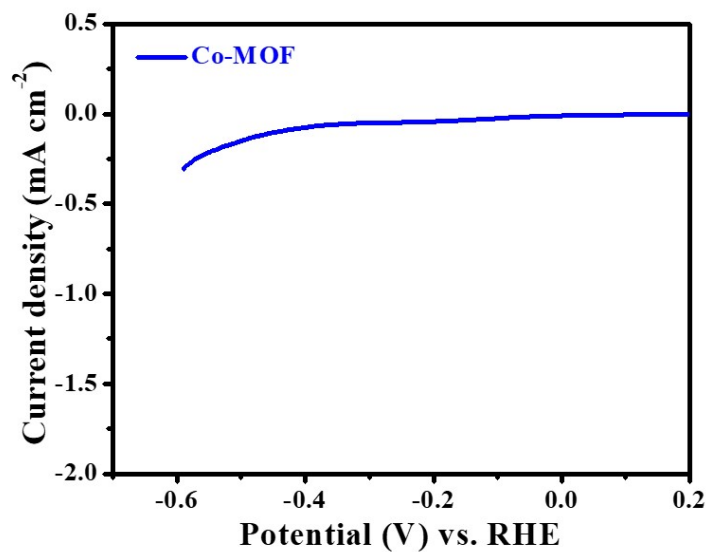

Fig. S13 Linear sweep voltammetry test for Co-MOF showing poor HER activity.
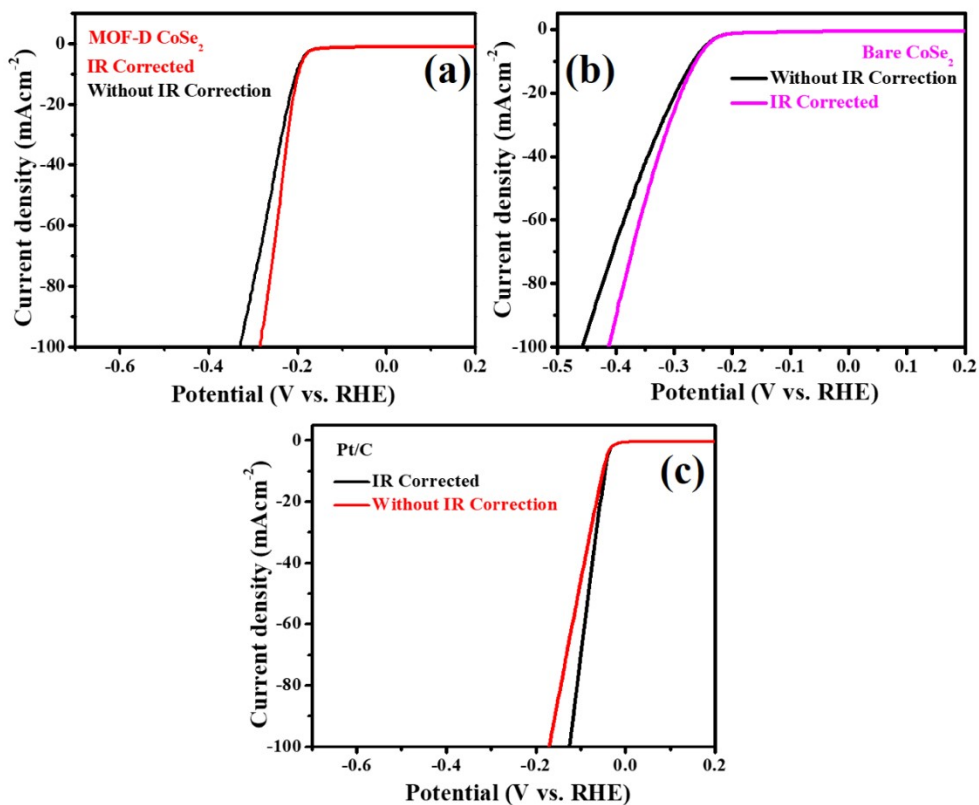
Fig. S14 Linear sweep voltammograms of (a) MOF-D CoSe₂, (b) bare CoSe₂ and (c) Pt/C for hydrogen evolution reaction before and after *iR* correction.
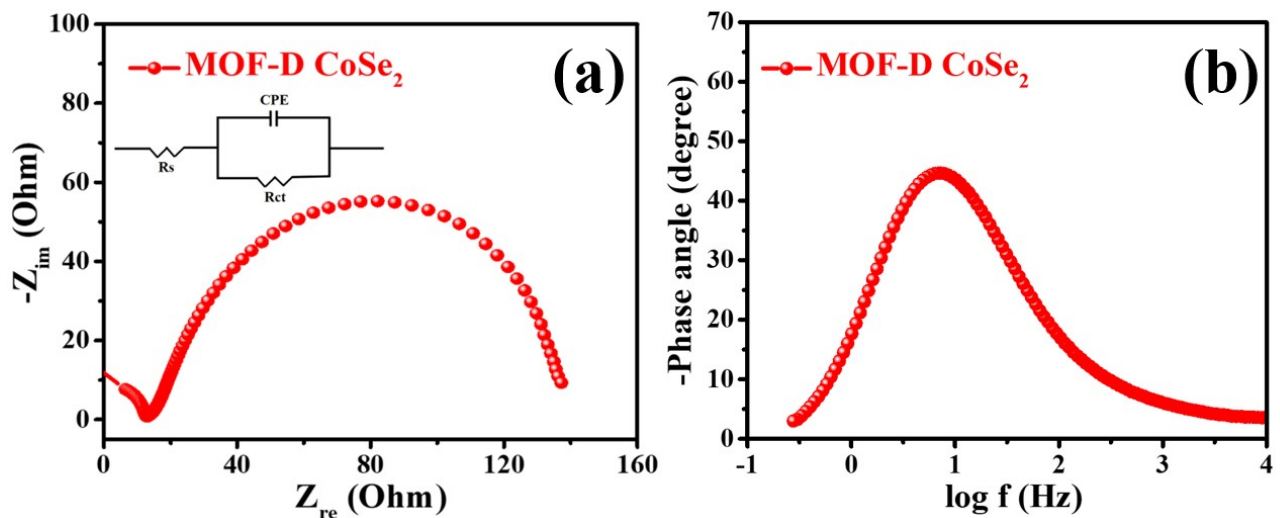

Fig. S15 (a) The equivalent circuit diagram of MOF-D CoSe₂ fitted to the obtained impedance result and (b) is the bode plot corresponds to the time constant for HER.

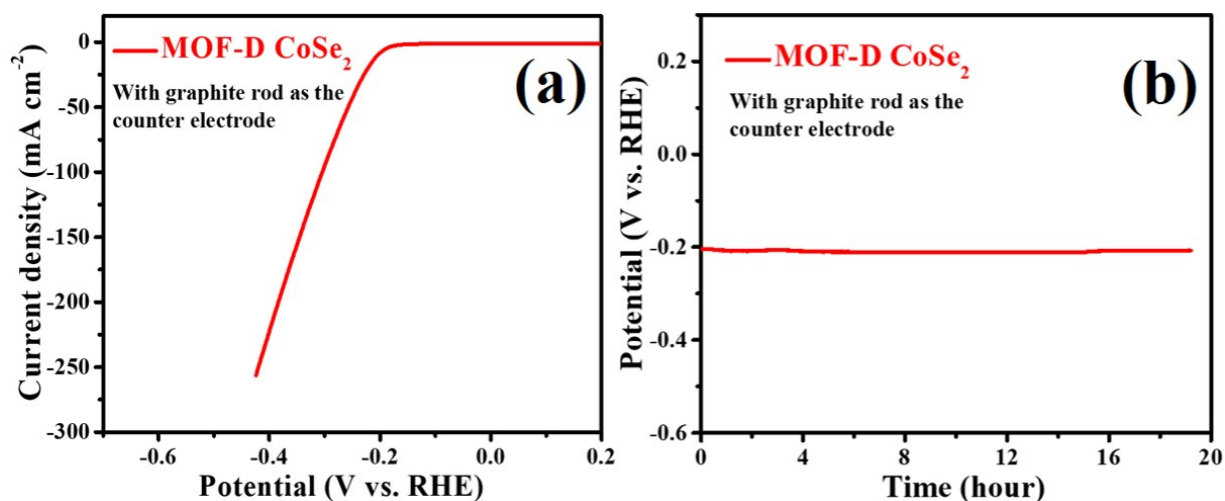**Fig. S16** (a) LSV plot of MOF-D CoSe$_2$ modified glassy carbon electrode for HER at 5 mV/s. (b) Stability test of MOF-D CoSe$_2$ at a current density of 10 mA/cm^2. Here graphite rod has been used as the counter electrode instead of platinum.
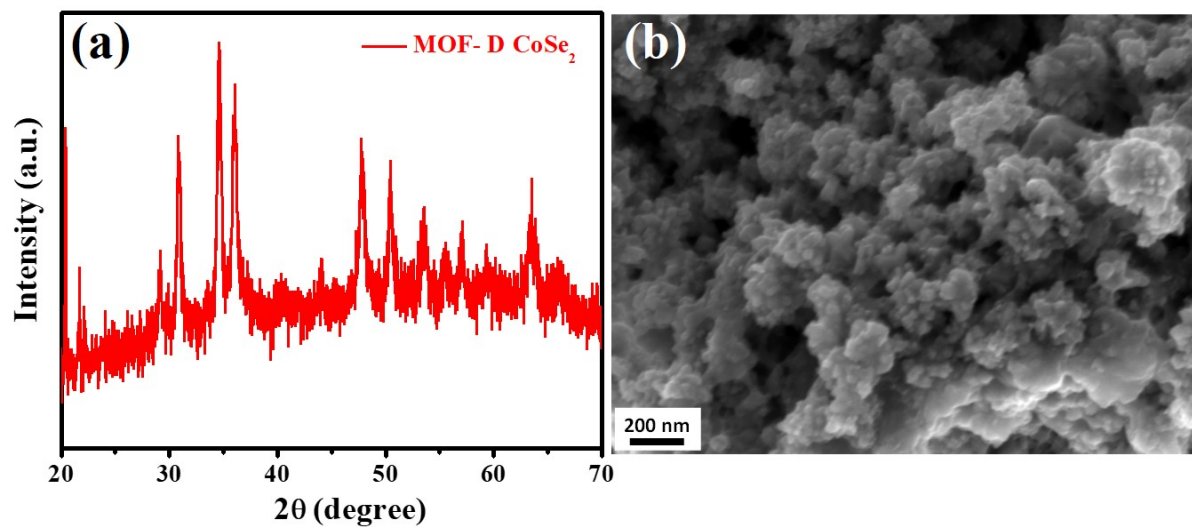
Fig. S17 (a) X-ray diffraction pattern and (b) FESEM image of MOF-D CoSe$_2$ after durability test for 19 hours in 0.5 M H$_2$SO$_4$ at 10 mA/cm^2.
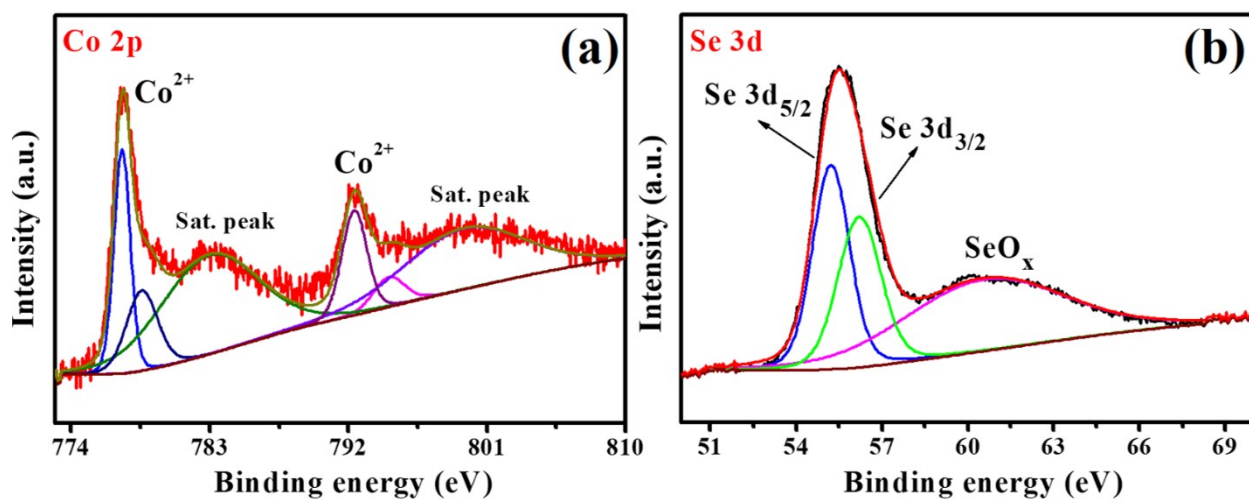
Fig. S18 (a, b) High-resolution XPS study of MOF-D $CoSe_2$ after 19 h of long-term stability test in 0.5 M H_2SO_4.
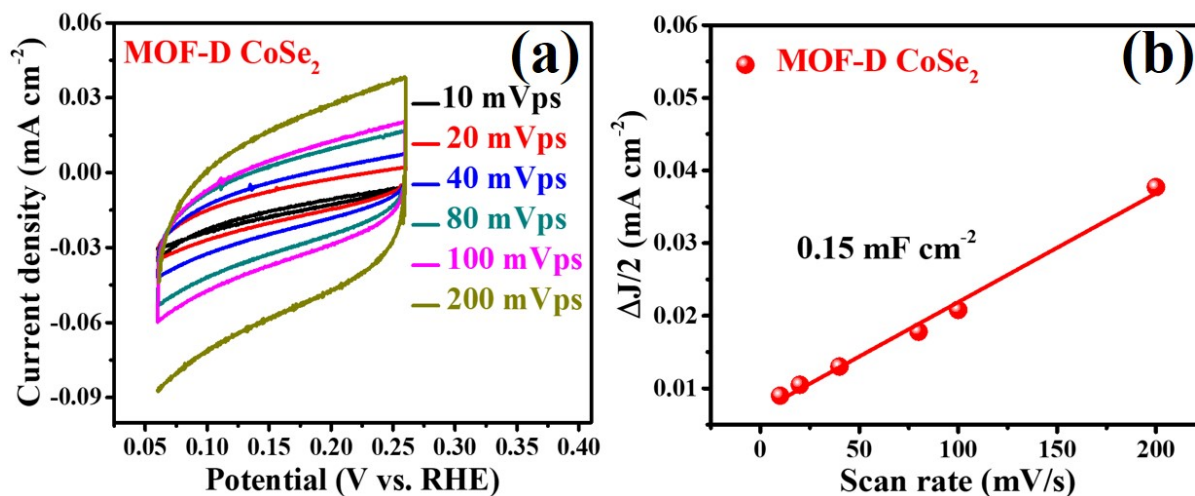
Fig. S19 (a) Cyclic voltammograms for MOF-D $CoSe_2$ in 0.5 M H_2SO_4 at different scan rates (from 10 to 200 mV/s) and (b) is the graph of current density at 0.16 (V vs. RHE) versus different scan rates to calculate C_{dl} of MOF-D $CoSe_2$.

Fig. S20 Powder X-ray diffraction of bare CoSe$_2$ (a) before electrolysis, (b, c) after electrolysis.

Table S1 OER Comparison table for MOF-D CoSe$_2$ with reported literature.

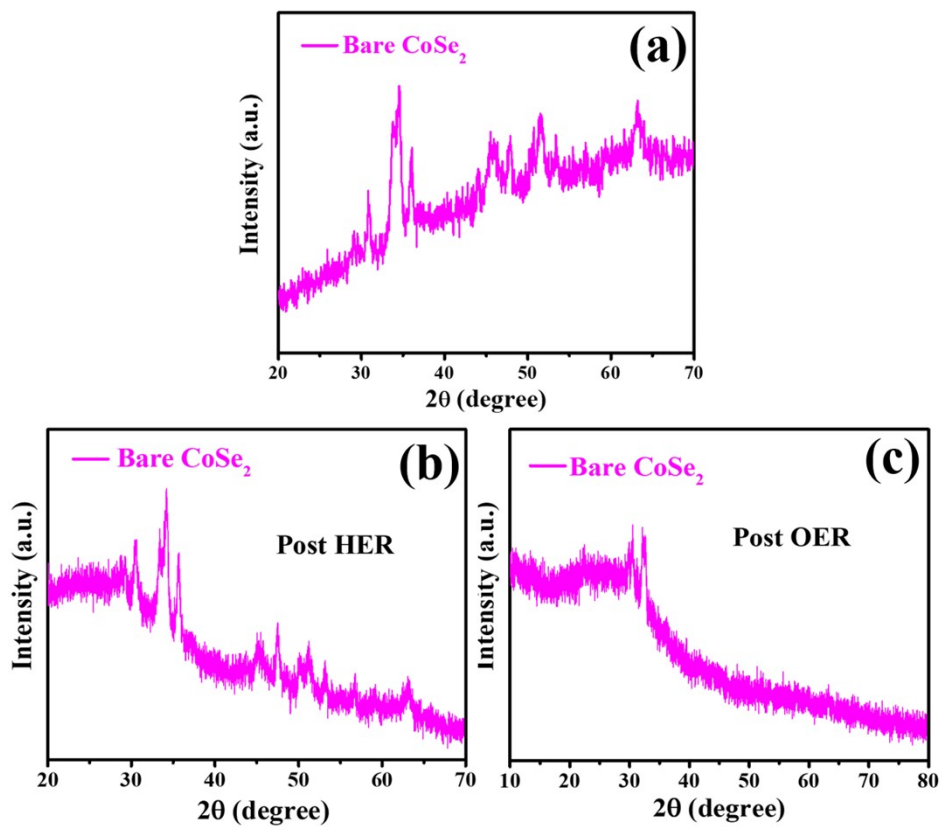| Serial Number	Sample	Over potential @10mA/cm^2	Tafel slope	Electrolyte used	References
1	CoSe$_2$-160 microcubes	328 mV	73.0 mV/dec	1 M KOH	Inorg. Chem. 2020, 59, 12778−12787
2	CoSe$_2$@N/C-CNT	340 mV	103.0 mV/dec	1 M KOH	J. Colloid Interf. Sci. 2020, 566, 296-303
3	CoSe$_2$-450 microspheres	330 mV	79.0 mV/dec	1 M KOH	J. Mater. Chem. A, 2017, 5, 15310-15314
4	CoSe$_2$/CNTs	324 mV	76.0 mV/dec	1 M KOH	Electrochim. Acta 2020, 331, 135362
5	Ni$_{0.88}$Co$_{1.22}$Se$_4$ hollow microparticles	320 mV	78.0 mV/dec	1 M KOH	Chem. Mater. 2017, 29, 7032-7041
6	hollow core-branch CoSe$_2$	320 mV	107.0 mV/dec	1 M KOH	Small 2018, 14, 1700979
7	CoSe$_2$@NC nanorods	310 mV	95.0 mV/dec	1 M KOH	J. Alloy. Compound 2019, 778, 134-140
8	FeCoSe$_2$/Co$_{0.85}$Se	330 mV	50.8 mV/dec	1 M KOH	J. Alloy. Compd. 2020, 825, 154073
9	Fe-doped CoSe$_2$@N-CT	330 mV	74 mV/dec	1 M KOH	Electrochim. Acta 2018, 265, 577-585
10	**Flower like MOF derived CoSe$_2$**	**320 mV**	**60 mV/dec**	**1M KOH**	**This Work**

Table S2. HER comparison table for flower shaped MOF-D CoSe$_2$ with reported data.

Serial Number	Sample	Over potential @10mA/cm^2	Tafel slope	Electrolyte used	References
1	CoSe$_2$-160 microcubes	156 mV	40.0 mV/dec	0.5 M H$_2$SO$_4$	Inorg. Chem. 2020, 59, 12778−12787
2	CoSe$_2$/C nanocrystals	260 mV	45.7 mV/dec	0.5 M H$_2$SO$_4$	Int. J. Hydrogen Energy 2020, 45, 1738-1747
3	CoSe$_2$ NP	250 mV	42.0 mV/dec	0.5 M H$_2$SO$_4$	Electrochim. Acta. 2017, 247, 258-264.
4	Ni$_{0.75}$Fe$_{0.25}$Se$_2$	197 mV	107 mV/dec	0.5 M H$_2$SO$_4$	Int. J. Hydrogen Energy, 2019, 44, 22796– 22805
5	CoSe$_2$ nanoparticle	196 mV	39.6 mV/dec	0.5 M H$_2$SO$_4$	Nanoscale, 2015, 7, 14813–14816
6	CoSe$_2$ nanosheet	247 mV	52.0 mV/dec	0.5 M H$_2$SO$_4$	J. Am. Chem. Soc. 2016, 138, 15, 5087–5092
7	CoSe$_2$@N/C-CNT	185 mV	98.0 mV/dec	0.5 M H$_2$SO$_4$	J. Colloid Interf. Sci. 2020, 566, 296-303
8	RGO/CoSe$_2$-180	172 mV	35.2 mV/dec	0.5 M H$_2$SO$_4$	Int. J. Hydrogen Energy, 2020, 45, 1738-1747
9	CoSe$_2$ spheres	167 mV	38.0 mV/dec	0.5 M H$_2$SO$_4$	J. Colloid Interf. Sci. 2019, 539, 646-653
10	**Flower like MOF derived CoSe$_2$**	**195 mV**	**43 mV/dec**	**0.5 M H$_2$SO$_4$**	**This Work**